Current **A**pplied **S**cience and **T**echnology e-ISSN: 2586-9396

Curr. Appl. Sci. Technol. 2025, Vol. 25 (No. 5), e0263917

Research article

Development of Orange-Emitting Sm_2O_3-Doped Tellurite Glasses Prepared for Solid State Lighting

Patarawagee Yasaka[1,2]*, Winut Wongwan[1,2], Kitipun Boonin[1,2], Warawut Sa-ardsin[3], Rungsan Ruamnikhom[4] and Jakrapong Kaewkhao[1,2]

[1]Center of Excellence in Glass Technology and Materials Science (CEGM), Nakhon Pathom Rajabhat University, Nakhon Pathom 73000, Thailand
[2]Physics Program, Faculty of Science and Technology, Nakhon Pathom Rajabhat University, 73000, Thailand
[3]Faculty of Science and Technology, Thepsatri Rajabhat University, Lopburi 15000, Thailand
[4]Faculty of Liberal Arts, Rajamangala University of Technology Rattanakosin, Nakhon Pathom, 73170, Thailand

Received: 6 July 2024, Revised: 25 November 2024, Accepted: 25 November 2024, Published: 28 March 2025

Abstract

A series of glass samples, with base composition of (40-x) TeO_2: $30B_2O_3$: 20ZnO: $10Li_2O$, was modified by incorporating varying concentrations of Sm_2O_3 (x = 0.00, 0.10, 0.50, 1.00, 1.50, and 2.00 mol%). X-ray diffraction analysis confirmed the amorphous nature of the prepared glasses. FTIR spectroscopy was used to investigate the structural arrangement of the glasses, revealing characteristic vibrational bands associated with Te-O, B-O, and Zn-O bonds. These bands provided insights into the glass network's evolution with changing Sm_2O_3 content. The optical properties of the glasses were investigated through absorption and photoluminescence studies. Absorption spectra, measured in the 400-1800 nm range, displayed seven peaks attributed to electronic transitions within the Sm^{3+} ion. These transitions originated from the $^6H_{5/2}$ ground state to various excited states. Photoluminescence analysis, excited at 403 nm, revealed a strong emission band centered at 597 nm. This emission corresponded to the $^4G_{5/2} \rightarrow {}^6H_{7/2}$ transition of Sm^{3+}, responsible for the characteristic orange luminescence. The emission intensity increased with increasing Sm_2O_3 concentration up to 1.00 mol%, after which concentration quenching led to a decrease in intensity. In conclusion, this study elucidates the composition-structure-property relationships in Sm_2O_3-doped TeO_2-B_2O_3-ZnO-Li_2O glasses. The tunable orange emission suggests their potential as phosphors for solid-state lighting applications, particularly in orange LEDs.

Keywords: glass; tellurite; luminescence; Sm_2O_3; solid-state lighting

*Corresponding author: E-mail: pyasaka@hotmail.com
https://doi.org/10.55003/cast.2025.263917

1. Introduction

Currently, rare earth (RE) ion-doped optical materials are garnering significant attention in the research community for their potential in solid-state lighting (SSL) applications. These materials possess several key advantages that make them highly attractive for a wide range of applications. Firstly, their reduced electricity consumption aligns with the growing demand for energy-efficient technologies, making them a sustainable choice. Secondly, their consistent performance ensures reliability and longevity, reducing maintenance costs and downtime. Thirdly, their minimal environmental impact addresses the increasing need for eco-friendly solutions. These attributes make them ideal for applications such as white LEDs for general lighting, traffic signals, vibrant full-color displays, high-density optical storage devices, clear display monitors, precise sensors, and efficient cellular phone illumination (Karthikeyan et al., 2017). Oxide glasses, due to their desirable physical, chemical, and thermal attributes, have been identified as the most reliable host materials for incorporating rare earth (RE) ions in practical technological applications. Furthermore, among the diverse types of oxide glasses, such as SiO_2, B_2O_3, and P_2O_5, tellurite glass is presently garnering substantial attention owing to its unique blend of attributes. These encompass a substantial light-bending capacity, remarkable resistance to heat and chemical reactions, effective heat transmission, and a relatively mild liquefaction point. It is worth noting that, under standard circumstances, tellurium oxide requires the addition of a modifying agent, such as alkali, alkaline earth, and transition metal oxides, or a substitute glass-forming compound, to effortlessly assume an amorphous, vitreous configuration (Khattak & Salim, 2002).

The inclusion of B_2O_3 in the composition facilitates glass formation due to its properties as a strong glass former, along with its high optical transparency, increased bond strength, good rare earth (RE) ion solubility, expanded glass-forming ability, and superior thermal stability. Furthermore, incorporating lithium oxide, an alkali metal known for its beneficial modifying effects, further enhances glass preparation processes. Research suggests that the introduction of zinc oxide (ZnO) enhances the water resistance properties of glass. The mechanism behind this is attributed to the Zn^{2+} ions functioning as ionic cross-linkers between phosphate anions, effectively hindering the hydration process (Takebe et al., 2006). Among rare earth elements, samarium (Sm^{3+} ion) demonstrates enhanced luminescence in the visible spectrum when incorporated into suitable glass matrices. Furthermore, its emission remains unaffected by high photonic energy, making samarium-doped glasses particularly appealing. These glasses are of particular interest due to the intense orange-red emission they exhibit in the visible region, a result of the $^4G_{5/2}$ transition of Sm^{3+} ions. Furthermore, the potential conversion of samarium ions from Sm^{3+} to Sm^{2+} states is significant, as Sm^{2+} ions possess strong emission bands within their d-orbital spectral region, opening up possibilities for a wider range of luminescence applications. This study concentrates on the fabrication of samarium-doped lithium zinc boro-tellurite glass using the melt quenching method. This investigation was aimed to analyze its physical, structural, optical, photoluminescence, and X-ray-induced luminescence characteristics to assess its potential for development and application in solid-state lighting (SSL) or as scintillator materials.

2. Materials and Methods

The (40-x) TeO_2: $30B_2O_3$: 20ZnO: $10Li_2O$: xSm_2O_3 (where x is 0.00, 0.10,0.50,1.00,1.50 and 2.00 mol%) were synthesized by the melting quenching technique. The process of glass synthesis began with weighing chemicals TeO_2 (99.8%), ZnO (99.0%), H_3BO_3(99.8%), Li_2CO_3 (99.5%), and Sm_2O_3 (99.99%) in quantities totaling 10 g, into an alumina crucible according to their respective compositional ratios. The combined chemicals were then melted at 1100°C and subsequently poured onto a graphite mold. Following this, the glass was annealed and allowed to gradually cool to ambient temperature, as illustrated in Figure 1. The resulting glasses were then cut and polished to dimensions of 1 cm x 1.5 cm x 0.3 cm to facilitate the measurement of their physical, optical, structural, and luminescence properties, as depicted in Figure 2. The glasses were analyzed in terms of their density (ρ) by density measurement kit (4 digit Microbalance), refractive index (*n*) by Presidium Refractive Index meter II, X-ray diffraction (XRD) by Shimadzu X-ray diffractometer -6100 (structural analysis of material/powder sample) at 40 kV and a tube current of 30 mA, Fourier transform infrared spectroscopy (FTIR) by Nicolet IS5 infrared spectroscopy measurement in the range of 400- 4000 cm^{-1}, Synchrotron X-ray photoelectron spectroscopy (XPS), absorption spectra by UV-VIS-NIR Spectrophotometer Shimadzu UV-3600 (A, %T, %R measurements in the range of 200-3300 nm), photoluminescence and lifetime by Fluorescence Spectrophotometer Cary-Eclipse (measurement of material in visible region from 200-900 nm) to investigate the possibility of using them in the synthesis of solid state lighting materials.

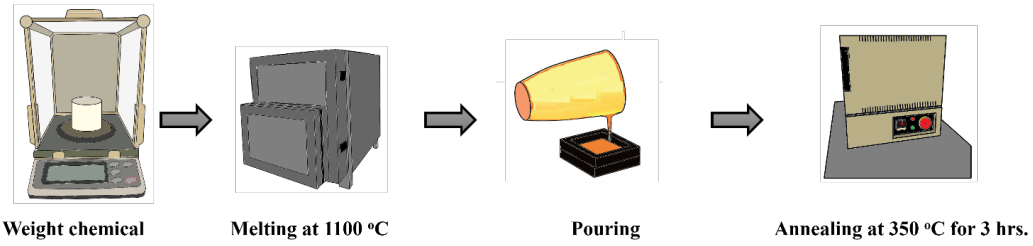

Figure 1. Illustration of the melt-quenching synthesis process for lithium zinc barium boro-tellurite glass doped with Sm^{3+} ions

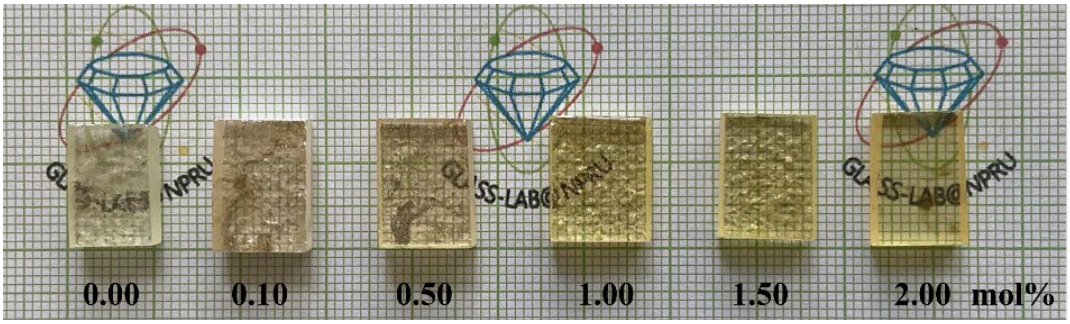

Figure 2. The lithium zinc barium boro-tellurite glass at different concentrations of Sm_2O_3

3. Results and Discussion

3.1 Density molar volumes and refractive index

The density, molar volume, and refractive index of lithium zinc barium boro-tellurite glass varied with Sm_2O_3 concentration (Figure 3). The density of glasses measured by the Archimedes principle from these equations:

$$\rho_{glass} = \frac{W_A}{W_A - W_w} \times \rho_w$$

Where W_A is the weight of the glass in air, W_w is the weight of the glass in distilled water, and ρ is the density of distilled water (~ 1 g/cm^3). The density of the glass was measured at least three times, and the average was calculated. The molar volume ($V_m = M_T/\rho$) of the glass samples is equal to the molecular weights (M_T) divided by the densities (ρ). As Sm_2O_3 content increases within the glass matrix, the density rises while the molar volume decreases. This inverse relationship between density and molar volume indicates a higher compactness in the developed glass samples. This is attributed to the substitution of TeO_2 (density 5.67 g/cm^3) with the denser Sm_2O_3 (density 8.35 g/cm^3). Additionally, the refractive index of the samples increases with higher Sm_2O_3 concentration, aligning with the density trend. This correlation arises because the increased compactness of the glass samples slows down the speed of light, thereby raising the refractive index.

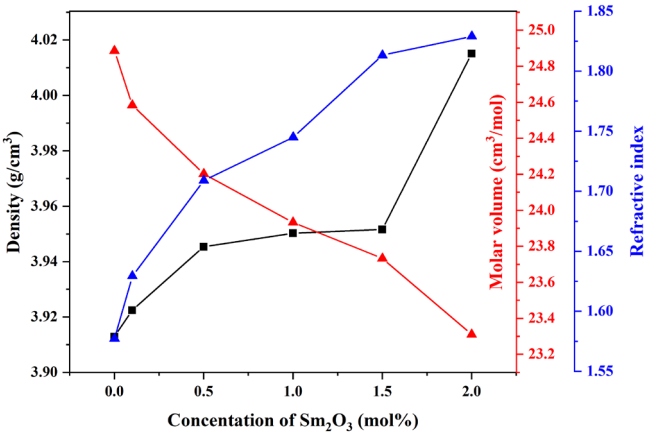

Figure 3. The density, molar volumes, and refractive index of prepared glasses

3.2 X-ray diffraction (XRD) and Fourier transform infrared

The X-ray diffraction (XRD) pattern was investigated in the range of 10° to 80°. The XRD pattern of the glasses is displayed in Figure 4. It shows broad scattering at lower angles, with no sharp peaks, revealing a non-crystalline nature. The infrared absorption spectrum of the glass samples, illustrated in Figure 5, was meticulously examined across a wavenumber span of 400-4000 cm^{-1}. Four well-defined absorption bands were identified at

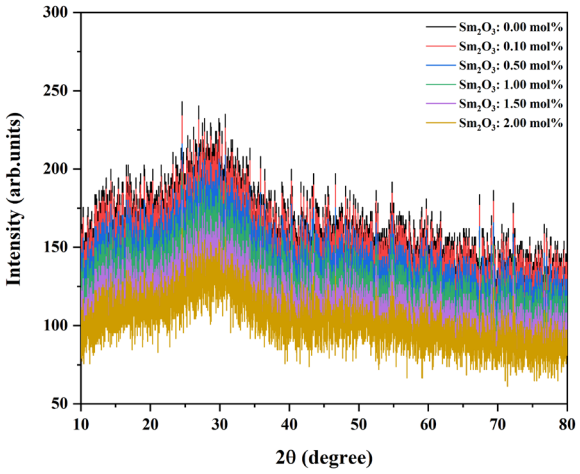

Figure 4. The X-ray diffraction of prepared glasses

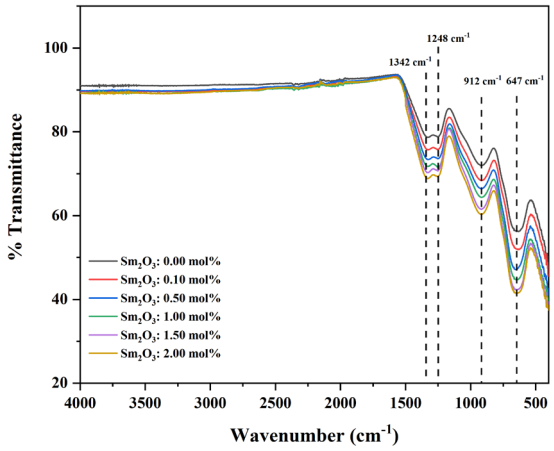

Figure 5. The Fourier transforms infrared spectra of prepared glasses

647, 912, 1248, and 1342 cm^{-1} (Table 1). The band situated at 647 cm^{-1} is ascribed to the flexing motions of Te-O bonds within the TeO_3 and TeO_6 structural building blocks. The absorption noted at 912 cm^{-1} is indicative of the stretching motions of B-O bonds in BO_4 units. The more expansive region between 1100 and 1500 cm^{-1} encompasses the stretching vibrations of B-O bonds in BO_3 units. Furthermore, the faint vibrations detected beyond 2000 cm^{-1} are probably attributable to the existence of OH groups. These spectral nuances provide glimpses into the transformations within the glass network framework. The emergence of truncated chains or a diminution in the mean chain length can be ascribed to the elongation oscillations of Te-O or B-O bonds linked with lone oxygen (NBO) atoms residing in diverse borate and tellurite assemblages. These structural metamorphoses become evident as a decline in the strength of the corresponding absorption peaks. Essentially, the infrared spectrum functions as a distinctive signature, unveiling the intricate structural rearrangements transpiring within the glass network owing to the interplay of disparate bond vibrations and the sway of unbonded oxygen atoms.

Table 1. The Fourier transforms infrared spectra and vibrations assignment

Wavenumber (cm^{-1})	Assignment	Ref.
647	The Te-O bending vibrations of TeO_3 and TeO_6 structural units	(Selvi et al., 2017)
912	The stretching vibrations of BO_4 units	(Rajaramakrishna et al., 2020)
1100-1500	The stretching vibrations of BO_3 units	(Rajaramakrishna et al., 2020)
> 2000	Vibration of OH groups	(Selvi et al., 2017)

3.3 Absorption spectra

The light absorption profiles of the synthesized glass specimens were meticulously measured at ambient temperature spanning wavelengths from 200 to 1800 nm utilizing a Shimadzu UV-3600 UV-VIS-NIR spectrophotometer. The resultant spectra, illustrated in Figure 6, disclosed eight distinct absorption maxima at 403, 472, 947, 1088, 1241, 1387, 1489, and 1527 nm. These peaks are ascribed to energy transitions within the Sm^{3+} ions, originating from their baseline energy state ($^6H_{5/2}$) to various elevated energy states, specifically $^4F_{7/2}$, $^4I_{13/2}$, $^6F_{11/2}$, $^6F_{9/2}$, $^6F_{7/2}$, $^6F_{5/2}$, $^6F_{3/2}$, and $^6H_{15/2}$, respectively. Notably, a direct correlation was observed between the intensity of the absorption spectra and the concentration of Sm^{3+} ions within the glass matrix. This phenomenon is attributed to the shielding effect exerted by the outermost electrons on the 4f electrons of rare earth (RE) ions, thereby influencing their interaction with incident light (Rani et al., 2020).

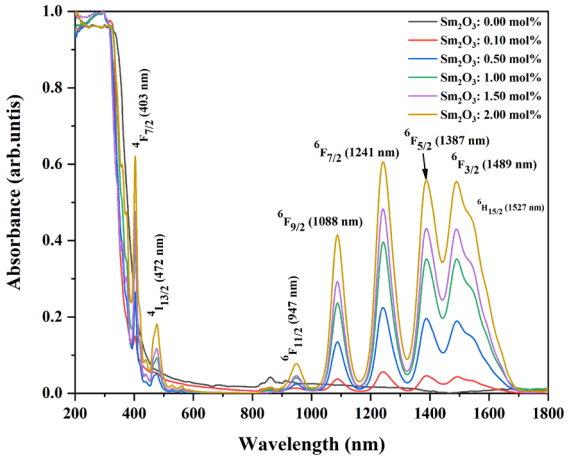

Figure 6. The absorption spectra of lithium zinc barium boro-tellurite glass doped Sm^{3+} ion

3.4 Photoluminescence studies

The excitation profiles of the prepared samples, measured at ambient temperature with a 598 nm emission wavelength, are depicted in Figure 7(a). Eight distinct excitation maxima were detected, situated at 345, 362, 375, 403, 417, 438, 462, and 474 nm. These peaks

are attributed to the transitions of Sm^{3+} ions from their fundamental energy state ($^6H_{5/2}$) to a variety of elevated energy levels ($^4K_{17/2}$, $^4D_{3/2}$, $^6P_{7/2}$, $^4F_{7/2}$, $^6P_{5/2}$, $^4G_{9/2}$, $^4I_{13/2}$, $^4I_{11/2}$, $^4G_{7/2}$, and $^4F_{3/2}$, correspondingly). The existence of these excitation maxima corroborates the successful integration of Sm^{3+} ions into the vitreous matrix and their capacity to assimilate energy at these particular wavelengths. Figure 7(b) portrays the emission spectra of the specimens under 403 nm excitation. Four emission peaks were discerned at 563, 598, 644, and 706 nm, aligning with transitions from the energized $^4G_{5/2}$ state to the lower energy levels of $^6H_{5/2}$ (yellow), $^6H_{7/2}$ (orange), $^6H_{9/2}$ (orange-reddish), and $^6H_{11/2}$ (red), respectively. The most prominent emission peak was situated at 598 nm, ascribed to the $^4G_{5/2} \rightarrow {}^6H_{7/2}$ transition. This vibrant orange emission is a sought-after attribute for prospective applications in orange light-emitting diodes (LEDs). Intriguingly, the emission intensity of the samples did not exhibit a linear relationship with Sm_2O_3 concentration. Instead, a zenith in intensity was observed at 1.00 mol% Sm_2O_3, followed by a subsequent decline at higher concentrations. This phenomenon, termed concentration quenching, is attributed to non-radiative energy transfer between neighboring Sm^{3+} ions when they are situated in close proximity. At elevated concentrations, the mean separation between Sm^{3+} ions diminishes, thereby augmenting the likelihood of energy transfer via cross-relaxation or resonant energy transfer mechanisms. This heightened energy transfer ultimately leads to a reduction in the overall emission intensity (Zaman et al., 2016). The CIE chromaticity diagram can be used to calculate the color of any visible light emission, which is the standard for assigning colors to wavelengths (Zaman et al., 2016). The CIE chromaticity diagram (Figure 8) discloses the color coordinates of the 1.00 mol% Sm_2O_3-doped glass to be (0.59, 0.40), verifying the orange hue of the emission. This further supports the potential application of these glasses as orange phosphors in solid-state lighting devices. In addition, the researchers studied the luminescence lifetime or the average time that a material remains in its excited state before returning to the ground state and emitting light (photons). The luminescence lifetime was analyzed at the emission wavelength of 598 nm, corresponding to the transition of Sm^{3+} ions at $^4G_{5/2} \rightarrow {}^6H_{7/2}$ under the excitation at 403 nm. The luminescence decay curve is well-fitted using a double exponential function. The following formula can determine the average luminescence lifetime.

$$\tau = \frac{A_1 \tau_1^2 + A_1 \tau_2^2}{A_1 \tau_1 + A_2 \tau_2}$$

Where A_1 and A_2 denote the amplitudes of respective decay components, and τ_1 and τ_2 are luminescence lifetime components contributing to the average lifetime. The results show that the average lifetimes of the prepared glasses are 1.432, 1.345, 0.971, 0.702, and 0.512 ms, which decrease with increasing Sm^{3+} concentration, as shown in Figure 9. This decrease is consistent with the observed concentration quenching effect and can be attributed to the increased probability of non-radiative energy transfer between Sm^{3+} ions at higher concentrations (Rajesh et al., 2020).

The Judd-Ofelt (JO) theoretical framework was employed to dissect the experimentally acquired oscillator strengths, enabling the determination of JO intensity parameters (Ω_2, Ω_4, and Ω_6) through a least-squares fitting methodology. A comprehensive discourse on the utilization of JO theory for assessing these parameters can be found in our prior publication (Rao et al., 2009). The computed JO parameters were subsequently utilized to calculate oscillator strengths (f_{cal}), which are presented in Table 2 alongside their experimental counterparts (f_{exp}). The marginal root-mean-square (rms) deviation observed

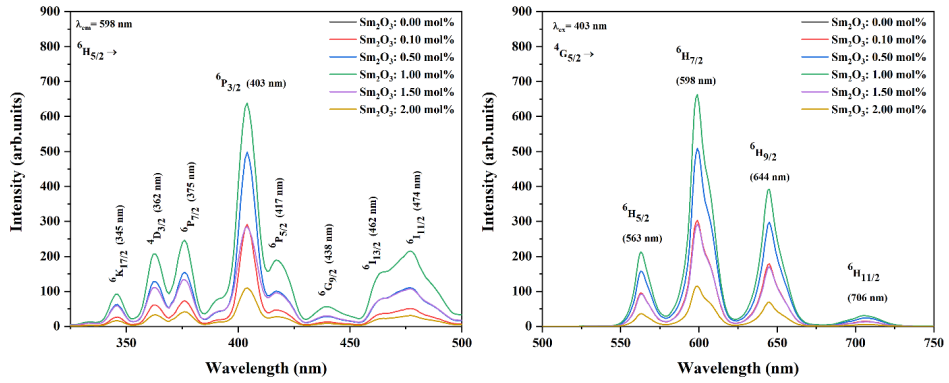

Figure 7. (a) The excitation spectra and (b) The emission spectra of prepared samples

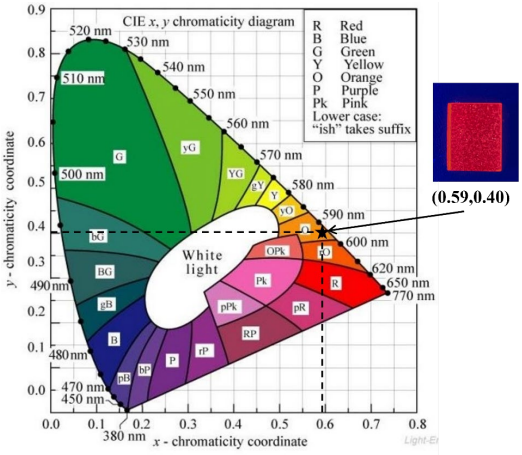

Figure 8. The CIE 1931 diagram of lithium zinc barium boro-tellurite glass doped Sm^{3+} ion

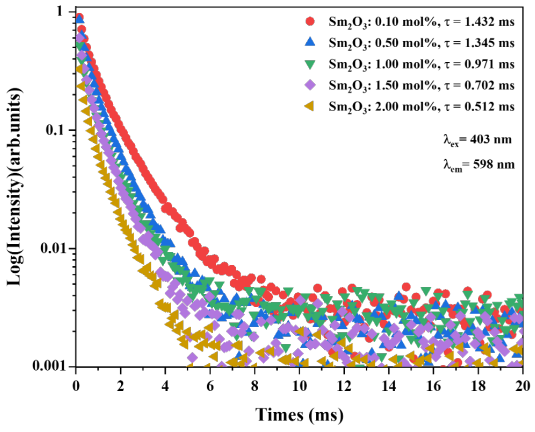

Figure 9. The lifetime of lithium zinc barium boro-tellurite glass doped Sm^{3+} ion

Table 2. Composition of Judd-Ofelt (JO) intensity parameters Ω_2, Ω_4, and Ω_6 ($\times 10^{-20}$ cm^2) of lithium zinc barium boro-tellurite glass doped 1.00 mol% of Sm_2O_3

Transition	λ (nm)	f_{exp} ($\times 10^{-6}$)	f_{cal} ($\times 10^{-6}$)
$^4F_{7/2}$	403	1.5479	3.995
$^4I_{13/2}$	472	0.3887	1.956
$^6F_{11/2}$	947	0.0121	0.4714
$^6F_{9/2}$	1088	0.5658	2.8697
$^6F_{7/2}$	1241	0.8912	4.0876
$^6F_{5/2}$	1387	0.3334	0.4238
$^6F_{3/2}$	1489	0.3861	0.7994
$^6H_{15/2}$	1527	0.1426	0.2401
σ_{rms}		±0.261	
Ω_2 ($\times 10^{-20}$) cm^2		4.71	
Ω_4 ($\times 10^{-20}$) cm^2		5.66	
Ω_6 ($\times 10^{-20}$) cm^2		6.16	

between the experimental and calculated oscillator strengths suggests a harmonious agreement and substantiates the applicability of JO theory within this context. Conventionally, the Ω_2 parameter is significantly influenced by the immediate environment surrounding the RE^{3+} ions, often exhibiting a correlation with factors such as the degree of asymmetry in the arrangement of coordinating atoms, the susceptibility of ligand ions to electronic distortion (polarizability), and the inherent character of chemical bonding. Conversely, Ω_6 displays a reciprocal relationship with the extent of electron sharing in Sm-O bonds, a characteristic that can be meticulously adjusted by modifying the composition or structural arrangement of the glass matrix. In contrast to both Ω_2 and Ω_6, the Ω_4 parameter is dependent upon macroscopic properties like the flow resistance (viscosity) and stiffness (rigidity) of the host material in which the ions are embedded (Kesavulu et al., 2016). These JO intensity parameters furnish invaluable insights into the local environment and bonding attributes of the Sm^{3+} ions ensconced within the lithium zinc barium boro-tellurite glass matrix. In this particular investigation, the JO parameters adhered to the pattern $\Omega_2 > \Omega_4 > \Omega_6$ for the 1.00 mol% Sm_2O_3-doped glass. This arrangement, particularly the heightened magnitude of Ω_2, signifies a greater degree of covalency and asymmetry in the ligand fields enveloping the Sm^{3+} ions (Rao & Jayasankar, 2013). In essence, this implies that the Sm^{3+} ions engage in more robust interactions with the surrounding glass network, culminating in a deformation of their electronic orbitals. These Judd-Ofelt (JO) intensity parameters are pivotal in assessing various radiative characteristics of the Sm^{3+} ions, encompassing the likelihood of spontaneous emission (radiative transition probability, A_R), the relative distribution of emitted light among different transitions (radiative branching ratio, β_R), and the effective areas presented by the ions for stimulated emission (stimulated emission cross-section, σ_e). These properties are succinctly summarized in Table 3. Notably, the experimental branching ratios (β_{Rexp}), derived by integrating the intensity of emission lines originating from the $^4G_{5/2}$ excited state, were juxtaposed with the predicted values (β_{Rcal}) gleaned from Judd-Ofelt theory. The branching ratio quantifies the relative apportionment of emission intensities among disparate transitions. A branching ratio surpassing 0.5 signifies that the majority of emission radiation is concentrated within a specific transition, thus rendering it a promising contender for laser applications. Table 3 unveils that the $^4G_{5/2} \rightarrow {}^6H_{7/2}$ transition exhibits the most elevated radiative transition rates in comparison to other transitions. This finding, coupled with the observation that the

Table 3. Emissions peaks (λ), radiative transition probabilities (A_R), stimulated emission cross-sections (σ_e), and experimental (exp.) and calculated (cal.) branching ratios (β_R) for the present work with comparison to other reported work

Transition ($^4G_{5/2}\rightarrow{}^6H_{7/2}$)	λ (nm)	A_R (s^{-1})	σ_e ($\times10^{-22}$) cm^2	β_{Rcal}	β_{Rexp}
Present work	598	281.3	1.05	0.54	0.53
KABPSm5 (Kiwsakunkran et al., 2018)	597	79.55	5.13	0.40	0.50
PKFBASm (Suhasini et al., 2009)	597	99.00	5.92	0.56	0.42
CdBiB (Sailaja et al., 2013)	600	325.11	6.95	0.57	0.43
SFB glass (Umamaheswari et al., 2012)	600	138.00	4.90	0.42	0.50

experimental branching ratio for this transition aligns harmoniously with the theoretical prediction, underscores its suitability for both solid-state lighting (SSL) and laser applications. The dominance of the $^4G_{5/2}\rightarrow{}^6H_{7/2}$ transition is consistent with the observed orange emission (centered at 598 nm) in the photoluminescence spectra, further solidifying the potential of these Sm^{3+}-doped glasses as orange-emitting phosphors or gain media for lasers.

4. Conclusions

Glasses with the composition (40-x) TeO_2: $30B_2O_3$: 20ZnO: $10Li_2O$: xSm_2O_3 (where x varies from 0.00 to 2.00 mol%) were fabricated using the melt quenching method, which rapidly cools the material. As the concentration of Sm_2O_3 increased, the glass density rose, while its molar volume decreased. The refractive index also increased with higher Sm_2O_3 concentrations, indicating that the glass could bend light more effectively. X-ray diffraction (XRD) confirmed that the glasses were amorphous (non-crystalline). Infrared absorption spectroscopy (FTIR) identified four distinct absorption bands at 647, 912, 1248, and 1342 cm^{-1}, corresponding to bending vibrations of Te-O bonds and stretching vibrations of BO_3 and BO_4 units, providing insight into the glass network's atomic structure. Absorption spectra revealed eight peaks corresponding to energy transitions of Sm^{3+} ions from their ground state to various excited states. The intensity of these peaks increased with higher Sm^{3+} concentrations, but concentration quenching occurred at 1.00 mol% Sm_2O_3, where further increases led to a reduction in absorption intensity. The luminescence properties of these glasses were also studied. The emission spectra indicated a reddish-orange color with color coordinates (0.59, 0.40). The luminescence lifetime of the excited state responsible for this emission decreased as Sm^{3+} concentration increased, suggesting more energy transfer between ions. Judd-Ofelt (JO) intensity parameters, which reflect the local environment and bonding of Sm^{3+} ions, followed the pattern $\Omega_2 > \Omega_4 > \Omega_6$ in the glass with 1.00 mol% Sm_2O_3. This suggests more electron sharing and irregularity around the Sm^{3+} ions. Further analysis of the luminescence characteristics showed that the reddish-orange emission had the highest radiative transition rate, making these glasses particularly suitable for solid-state lighting (SSL). In conclusion, this study demonstrated that Sm_2O_3-

doped lithium zinc barium boro-tellurite glasses have strong potential as high-performance reddish-orange light-emitting materials for SSL. Their tunable properties and efficient emissions make them promising candidates for future optoelectronic devices.

5. Acknowledgements

The authors gratefully acknowledge the support provided by Nakhon Pathom Rajabhat University, which made this research possible. Furthermore, we extend our sincere thanks to the Center of Excellence in Glass Technology and Materials Science (CEGM) for granting us access to their state-of-the-art measurement facilities, without which this study would not have been feasible.

6. Conflicts of Interest

The authors declare that they have no known competing financial interests or personal relationships that could have influenced the work reported in this paper.

ORCID

Patarawagee Yasaka https://orcid.org/0000-0003-2392-046X.

References

Karthikeyan, P., Vijayakumar, R. & Marimuthu, K. (2017). Luminescence studies on Dy^{3+} doped calcium boro-tellurite glasses for white light applications. *Physica B: Condensed Matter*, 521, 347-354. https://doi.org/10.1016/j.physb.2017.07.018

Kesavulu, C. R., Kim, H. J., Lee, S. W., Kaewkhao, J., Wantana, N., Kothan, S. & Kaewjaeng, S. (2016). Influence of Er^{3+}ion concentration on optical and photoluminescence properties of Er^{3+}-doped gadolinium-calcium silica borate glasses. *Journal of Alloys and Compounds*, 683, 590-598. https://doi.org/10.1016/j.jallcom.2016.04.314

Khattak, G. D. & Salim, M. A. (2002). *X-ray photoelectron spectroscopic studies of zinc – tellurite glasses*. 123, 47-55.

Kiwsakunkran, N., Chanthima, N., Kaewkhao, J. & Sangwaranatee, N. (2018). Fabrication of potassium aluminium barium phosphate glasses doped with Sm^{3+} and their Judd-Ofelt analysis for orange lasing material application. *Materials Today: Proceedings*, 43, 2554-2562. https://doi.org/10.1016/j.matpr.2020.04.616

Rajaramakrishna, R., Kaewjaeng, S., Kaewkhao, J. & Kothan, S. (2020). Investigation of XANES study and energy transport phenomenon of Gd^{3+} to Ce^{3+} in $CaO–SiO_2–B_2O_3$ glasses. *Optical Materials*, 102 Article 109826. https://doi.org/10.1016/j.optmat.2020.109826

Rajesh, M., Reddy, G. R., Sushma, N. J., Devarajulu, G. & Raju, B. D. P. (2020). Phonon sideband analysis, structural and spectroscopic properties of Eu^{3+} ions embedded $SiO_2–B_2O_3–CaF2–NaF–Na_2O$ glasses. *Optical Materials*, 107, Article 110038. https://doi.org/10.1016/j.optmat.2020.110038

Rani, P. R., Venkateswarlu, M., Swapna, K., Mahamuda, S., Prasad, M. V. V. K. S. & Rao, A. S. (2020). Spectroscopic and luminescence properties of Ho^{3+} ions doped barium lead alumino fluoro borate glasses for green laser applications. *Solid State Sciences*, 102, Article 106175. https://doi.org/10.1016/j.solidstatesciences.2020.106175

Rao, C. S & Jayasankar, C. K. (2013). Spectroscopic and radiative properties of Sm^{3+}-doped K-Mg-Al phosphate glasses. *Optics Communications*, 286, 204-210.

https://doi.org/10.1016/j.optcom.2012.08.042

Rao, A. S., Rao, B. R. V., Prasad, M. V. V. K. S., Kumar, J. V. S., Jayasimhadri, M., Rao, J. L. & Chakradhar, R. P. S. (2009). Spectroscopic and optical properties of Nd^{3+} doped fluorine containing alkali and alkaline earth zinc-aluminophosphate optical glasses. *Physica B: Condensed Matter*, 404(20), 3717-3721. https://doi.org/10.1016/j.physb.2009.06.114

Sailaja, S., Raju, C. N., Reddy, C. A., Raju, B. D. P., Jho, Y.-D. & Reddy, B. S. (2013). Optical properties of Sm^{3+}-doped cadmium bismuth borate glasses. *Journal of Molecular Structure*, 1038, 29-34. https://doi.org/10.1016/j.molstruc.2013.01.052

Selvi, S., Marimuthu, K. & Muralidharan, G. (2017). Effect of PbO on the B_2O_3–TeO_2–P_2O_5–BaO–CdO–Sm_2O_3 glasses - Structural and optical investigations. *Journal of Non-Crystalline Solids*, 461, 35-46. https://doi.org/10.1016/j.jnoncrysol.2017.01.028

Suhasini, T., Kumar, J. S., Sasikala, T., Jang, K., Lee, H. S., Jayasimhadri, M., Jeong, J. H., Yi, S. S. & Moorthy, L. R. (2009). Absorption and fluorescence properties of Sm^{3+} ions in fluoride containing phosphate glasses. *Optical Materials*, 31(8), 1167-1172. https://doi.org/10.1016/j.optmat.2008.12.008

Takebe, H., Baba, Y. & Kuwabara, M. (2006). Dissolution behavior of ZnO-P2O5 glasses in water. *Journal of Non-Crystalline Solids*, 352(28-29), 3088-3094. https://doi.org/10.1016/j.jnoncrysol.2006.04.002

Umamaheswari, D., Jamalaiah, B. C., Sasikala, T., Kim, I. G. & Moorthy, L. R. (2012). Photoluminescence properties of Sm^{3+}-doped SFB glasses for efficient visible lasers. *Journal of Non-Crystalline Solids*, 358(4), 782-787. https://doi.org/10.1016/j.jnoncrysol.2011.12.023

Zaman, F., Kaewkhao, J., Rooh, G., Srisittipokakun, N. & Kim, H. J. (2016). Optical and luminescence properties of Li_2O-Gd_2O_3-MO-B_2O_3-Sm_2O_3 (MO=Bi_2O_3, BaO) glasses. *Journal of Alloys and Compounds*, 676, 275-285. https://doi.org/10.1016/j.jallcom.2016.03.176